DOI: 10.1002/anie.201209363

Photoelectrochemical Water Splitting

Boron Carbides as Efficient, Metal-Free, Visible-Light-Responsive Photocatalysts**

Jikai Liu, Shuhao Wen, Yang Hou, Fan Zuo, Gregory J. O. Beran, and Pingyun Feng**

Solar-powered photocatalytic and photoelectrochemical (PEC) water splitting provide two promising strategies to produce hydrogen for future energy needs. Currently, most photocatalytic or PEC water-splitting materials are based on transition metal oxide, (oxy)nitride, or (oxy)sulfide semiconductors with suitable band gaps and band positions.[1] However, finding stable, efficient, and low-cost materials that are active under visible light has proved challenging.

Metal-free photocatalytic materials are a promising new class of photocatalytic materials that have not been fully explored. In 2009, a novel metal-free polymeric photocatalyst, graphitic C_3N_4 (g-C_3N_4),[2] was found to perform photocatalytic water splitting in the visible light region. The appealing electronic structure of this material, its chemical and physical stability, and its low cost make it potentially useful in a variety of applications.[3] However, few such metal-free photocatalysts are currently known: poly(*p*-phenylenes),[4] g-C_3N_4, $C_3N_3S_3$,[5] α-sulfur[6] and red phosphorus.[7] Unfortunately, all of these metal-free materials achieve sufficient efficiency only when loaded with scarce and expensive noble metal cocatalysts, as is also the case for PEC water splitting with these materials.[8] Moreover, although various *p*-type semiconductors exhibit sufficient efficiency as photocathode materials,[1c] their high cost and poor corrosion stability pose severe limitations on the potential application of these materials as photocathodes.

Herein, we demonstrate that stable and inexpensive boron carbides ($B_{4.3}C$ and $B_{13}C_2$), which are already used in large quantities for many industrial applications,[9] can also function as efficient visible-light-responsive photocatalysts for H_2 evolution. Critically, the H_2 evolution rate of $B_{4.3}C$ is about two orders of magnitude larger than that of g-C_3N_4, without the need for noble metal cocatalysts (ca. 2.9 μmol h^{-1}/0.2 g vs. ca. 0.035 μmol h^{-1}/0.2 g for g-C_3N_4 in the presence of sacrificial methanol). The apparent quantum yield of $B_{4.3}C$ is also higher: 0.54% of Pt/$B_{4.3}C$ vs. 0.23% of Pt/g-C_3N_4 at 420 nm. Furthermore, the *p*-type semiconducting nature of the boron carbides makes them one of only a handful of known stable and efficient photocathode materials for PEC water reduction under visible light irradiation that do not require noble metal cocatalysts.[10] Density functional theory (DFT) calculations indicate that the inherent defects and structural distortions in $B_{4.3}C$ cause a continuum downshift of its conduction band (CB) edge that facilitates visible-light absorption and water splitting. In $B_{13}C_2$, however, the more complicated structural defects and distortions result in a large number of midgap states between the CB and the valence band (VB), which reduce its overall photocatalytic and PEC water splitting efficiency by promoting charge recombination.

The commercially available "B_4C" used in this study is actually $B_{4.3}C$+free graphitic carbon.[11] The $B_{13}C_2$ was prepared by arc-melting crystalline boron with pure graphite under vacuum. Boron carbides have a rhombohedral structure with space group $R\bar{3}m$.[12] They are composed of B_{12} or $B_{11}C$ icosahedra, which distort slightly at each vertex owing to Jahn–Teller effects, and which are connected by mostly linear three-atom chains on the main cell diagonal (the crystallographic c direction).[13] Disordered combinations of the 12-atom icosahedra and three-atom chains (C-B-C, B-Vacancy-B, C-B-B) lead to elementary cells with different stoichiometric compositions which are statistically distributed over the whole structure.[14] The idealized boron carbide elementary cell is shown in Figure 1a.

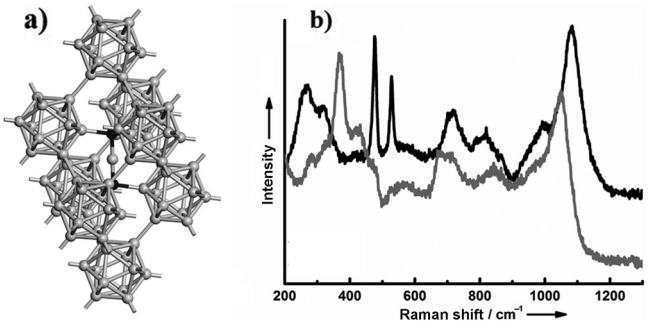

Figure 1. a) Idealized elementary cell of boron carbides. B gray, C black. b) FT-Raman spectra. $B_{13}C_2$ (gray), $B_{4.3}C$ (black).

The boron carbides were primarily evaluated by X-ray diffraction (XRD), FT-Raman spectroscopy, photoluminescence (PL) spectroscopy, scanning electron microscopy (SEM), and energy-dispersive X-ray spectroscopy (EDX). The XRD patterns (Supporting Information, Figure S3) match that of either $B_{4.3}C$ or $B_{13}C_2$, although their identical crystal structures make it difficult to distinguish between

[*] J. Liu, Dr. S. Wen, Dr. Y. Hou, Dr. F. Zuo, Prof. G. J. O. Beran, Prof. P. Feng
Department of Chemistry, University of California
Riverside, CA 92521 (USA)
E-mail: gregory.beran@ucr.edu
pingyun.feng@ucr.edu

[**] This work was supported by the NSF (CHE-1213795 to P.F. for project initiation and performing experiments, and CHE-1112568 to G.B. for theoretical modeling). We thank Dr. Arron Pekker and Prof. Robert C. Haddon for the use of an FT-Raman instrument. This study was also supported with supercomputer time from XSEDE (TG-CHE110064) and from the Shanghai supercomputer center.

Supporting information for this article is available on the WWW under http://dx.doi.org/10.1002/anie.201209363.

them based on the XRD patterns. The small low-angle shift for $B_{13}C_2$ compared to $B_{4.3}C$ indicates that the former has larger unit cells, which is in agreement with previous results.[15] Both boron carbides contain a small amount of free graphitic carbon, which is rather common in both commercial boron carbides[13] and boron carbides synthesized by arc-melting.[16] However. the graphitic carbon is not active in either photocatalytic or PEC water splitting.

FT-Raman spectroscopy was used to further identify the two boron carbides. The FT-Raman spectra shown in Figure 1b are in good agreement with a previous FT-Raman study on various boron carbides.[17] Compared to $B_{4.3}C$, the two narrow bands near 500 cm^{-1} and the broad bands near 300 cm^{-1} disappear in our synthesized boron carbide, and a broad band near 370 cm^{-1} appears. These changes correspond to the replacement of C-B-C chains with C-B-B chains and indicate that the C content is 13% ($B_{13}C_2$) or lower.[17] However, B_xC with lower C content than $B_{13}C_2$ are unlikely here, because they would be metastable and would yield different crystal structures, such as B_8C (orthorhombic) or $B_{25}C$ (tetragonal), which would be inconsistent with the observed XRD pattern of the synthesized boron carbide.[18] Theoretical calculations of the enthalpies of formation for the ideal boron carbide structures also indicate that materials with the stoichiometries of B_4C and $B_{13}C_2$ have the lowest enthalpies of formation.[19] The combination of this evidence indicates that the synthesized boron carbide is $B_{13}C_2$.

Because of the dark coloration and high absorption coefficient of boron carbides, the powder samples show high absorption in the full region of 310–800 nm by UV/Vis diffuse reflectance spectroscopy (Figure S5a). Instead, PL spectroscopy was adopted to further elucidate the electronic structures of boron carbides. A peak centered at ca. 448 nm (2.78 eV) was observed with an excitation wavelength of 325 nm in Figure S5b. This agrees well with a previous theoretical study, and indicates that an indirect energy gap of 2.78 eV exists in $B_{12}C_3$.[20] SEM images (Figure S6) show that both boron carbides consist of big particles and the size varies from several micrometers to ca. 10 μm. The specific surface areas of both boron carbides are negligible by the Brunauer-Emmett-Teller (BET) method. EDX spectra (Figure S7) confirm that the photocatalysts only contain boron and carbon elements (the Cu and Pt elements are from the substrates and coating for EDX measurements). TGA analysis (Figure S11) shows that the boron carbides start being oxidized at ca. 450 °C in air.

The photocatalytic properties of boron carbides for H_2 evolution from water were studied using a 25% methanol aqueous solution as the sacrificial agent under visible light irradiation (> 420 nm). Figure 2 shows the time courses of H_2 evolution from the two boron carbides. Without any cocatalysts, the H_2 evolution rates (average rate from four cycles) of $B_{4.3}C$ and $B_{13}C_2$ are ca. 2.9 μmol h^{-1}/0.2 g and ca. 0.9 μmol h^{-1}/0.2 g, respectively. After loading 2 wt% Pt, the H_2 evolution rates of $B_{4.3}C$ and $B_{13}C_2$ were increased to ca. 6.2 μmol h^{-1}/0.2 g and ca. 1.6 μmol h^{-1}/0.2 g, respectively. The H_2 evolution rates remain stable even after 100 h (see the fourth cycle), which is indicative of long-term photocatalyst stability. For comparison, we studied metal-free g-C_3N_4 photocatalysts, which were synthesized according to a previous report.[2] The g-C_3N_4 catalyst exhibits ca. 0.035 μmol h^{-1}/0.2 g of H_2 evolution without Pt loading, and ca. 4.7 μmol h^{-1}/0.2 g after loading 2 wt% Pt (Figure S8). Therefore, $B_{4.3}C$ exhibits a rate of H_2 evolution ca. 83 times higher than that of g-C_3N_4 without Pt loading and 1.3 times higher than with 2 wt% Pt loading. The apparent quantum yield (AQY) of

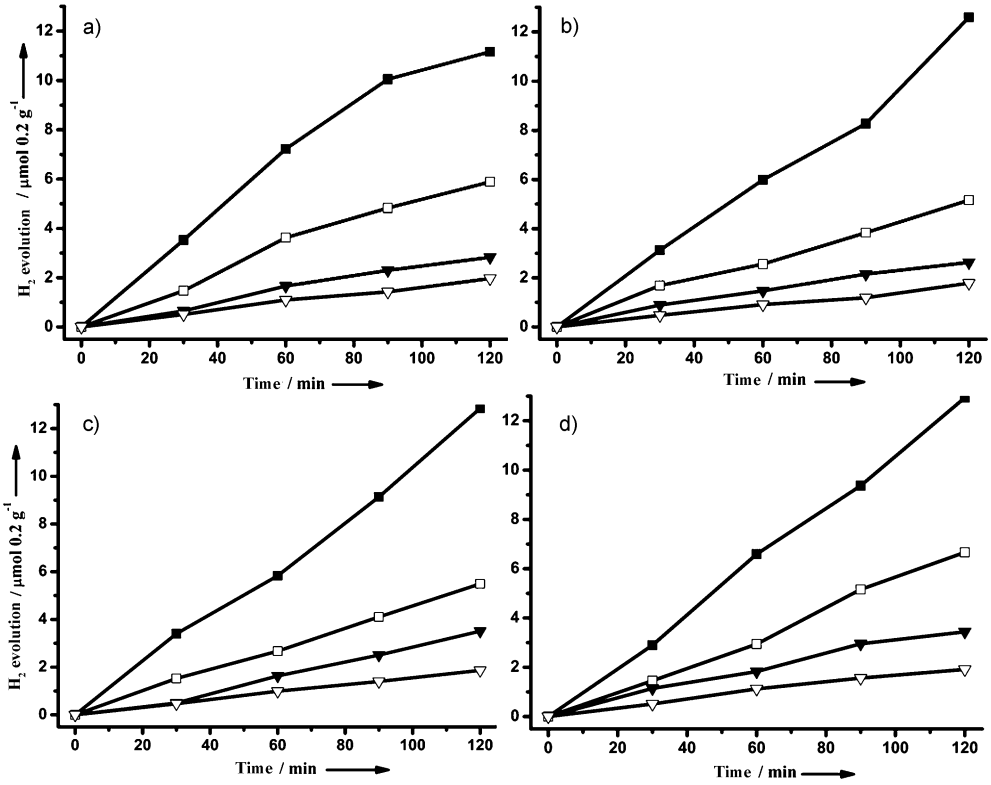

Figure 2. Time course of H_2 evolution under visible light irradiation. a) 1st cycle, b) 2nd cycle after re-evacuation, c) 3rd cycle after re-evacuation, d) 4th cycle after re-evacuation and 100 h reaction time. $B_{4.3}C$ with Pt(——■——), $B_{4.3}C$ without Pt(——□——), $B_{13}C_2$ with Pt(——▼——), $B_{13}C_2$ without Pt(——▽——).

$B_{4.3}C$ and g-C_3N_4 was determined with a 420 nm band-pass filter (see the Supporting Information). The observed AQY of Pt/$B_{4.3}C$ is ca. 0.54% compared to ca. 0.23% of Pt/g-C_3N_4 at 420 nm (AQY of bare $B_{4.3}C$ is ca. 0.34%). The water splitting reactions proceeded catalytically, as indicated by calculated turnover numbers of greater than 2 (generated H_2 to amount of photocatalysts used; see the Supporting Information). To facilitate the measurements, H_2 was collected by illuminating the reaction using a 300 W Xe lamp without any filter.[2] After the turnover experiments, the photocatalysts were centrifuged and recharacterized by XRD and FT-Raman spectroscopy to confirm the photostability of boron carbides. Aside from a slight decrease in the XRD peak intensities for $B_{4.3}C$, there are no obvious changes in the peak positions of XRD or FT-Raman spectra, as shown in Figures S3b and S4a. This indicates that the crystalline structure of $B_{4.3}C$ is preserved after the turnover experiments and that $B_{4.3}C$ is stable during the reaction process. After the photocatalytic reactions, the $B_{13}C_2$ XRD peak at ca. 31.8° disappeared and the Raman spectra shifted to slightly higher wavenumbers (Figures S3c and S4b), which indicates that there were some structural changes of $B_{13}C_2$. However, the main crystal structure of $B_{13}C_2$ is still maintained after the photocatalytic reactions. The overall peak intensity decrease may be due to the peak broadening associated with the reduced sample particle size resulting from the constant stirring during photocatalysis.

The PEC experiments were conducted with boron carbide films on fluorine-doped tin-oxide glass slides (FTO) prepared by electrophoretic deposition (EPD) under optimized experimental conditions (see the Supporting Information). This procedure is commonly employed in the processing of ceramics, coatings, and composite materials.[21] For each photocathode, a significant cathodic photocurrent was observed that increased with increasing negative potential bias, thus indicating their *p*-type characteristics in the depletion condition. Figure 3a shows the current-density-potential (J-E) behavior of the boron carbide films in aqueous Na_2SO_4 solution (0.01M) both in the dark and under visible light irradiation (> 420 nm). The electrode achieves a cathodic current density of ca. 46 μA cm^{-2} for $B_{4.3}C$ and ca. 16 μA cm^{-2} for $B_{13}C_2$ at −0.8 V applied bias vs. SCE (after subtracting dark current) as shown in Figure 3b.

DFT calculations were performed to understand the different observed photocatalytic behaviors of the two boron carbides. Because boron carbides exhibit an extremely high concentration of defects,[22] no single unit cell can adequately represent the whole structure. Fortunately, the concentrations of structural defects (B_{12} and $B_{11}C$ icosahedra; C-B-C, C-B-B, B-vacancy-B chains) in boron carbides have been studied in detail.[14] To model these materials with periodic DFT calculations, we constructed $5 \times 1 \times 1$ supercell models for $B_{4.3}C$ and $B_{13}C_2$, into which we can introduce defects in roughly the same proportions as in the experimental materials. Specific details on the structures and DFT calculation procedures are provided in the Supporting Information.

We then computed the density of states (DOS) of $B_{4.3}C$ and $B_{13}C_2$ for 1) idealized, geometry-optimized boron carbides without defects, (such as $(B_{11}C)CBC$), 2) boron carbides with defects inserted with no geometric relaxation, and 3) fully relaxed defect-containing boron carbides (Figure 4). First, our computed DOS on the idealized models agrees well with previous reports (Figure S9).[22] Second, the high concentration of structural defects distorts the B_{12} or $B_{11}C$ icosahedra in $B_{4.3}C$ and $B_{13}C_2$ upon DFT supercell optimization (Figure S1 and S2).

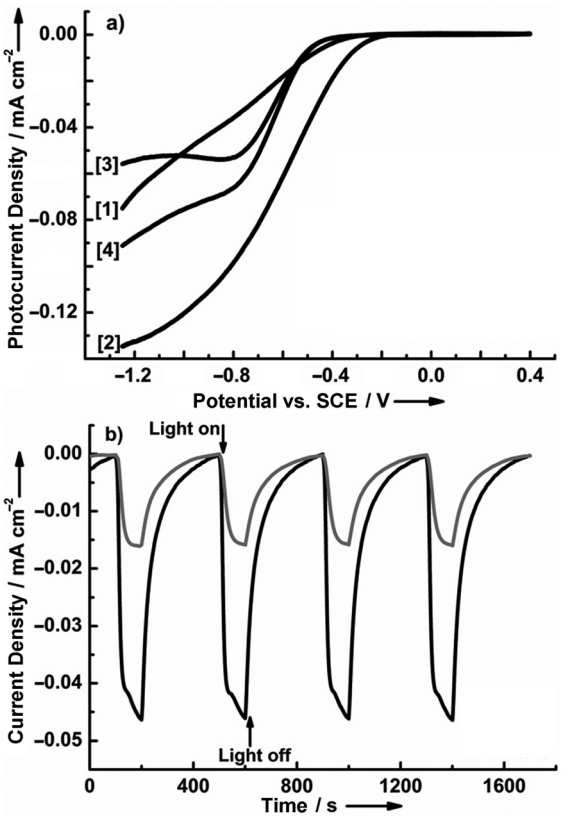

Figure 3. a) Current-potential curves in Na_2SO_4 aqueous solution (0.01 M) under visible light. [1] $B_{4.3}C$ dark, [2] $B_{4.3}C$ visible light, [3] $B_{13}C_2$ dark, [4] $B_{13}C_2$ visible light. b) Transient photocurrent curves under visible light at −0.8 V vs. SCE. $B_{13}C_2$ (gray), $B_{4.3}C$ (black).

As shown in Figure 4, significant changes in the DOS occur when the defects are introduced, and larger changes appear once the defect-containing structures are relaxed. In $B_{4.3}C$, the fully relaxed, defect-containing structure exhibits a significant continuum downshift of the CB and new midgap states at the Fermi level (see Figure 4e). As shown in Figures 4 and S10, the CB edge downshift arises from distortions of the $B_{11}C$ and B_{12} icosahedra upon structural relaxation, whereas the midgap state arises from the C-B-B chain defect. As a result, compared to the idealized structure, the intrinsic defects in $B_{4.3}C$ narrow the band gap from ca. 3.0 eV to ca. 2.1 eV and facilitate its visible light absorption. Similarly, previous studies which demonstrated that introducing significant surface disorder by hydrogenating TiO_2[23] or growing a new phase on the surface of rutile TiO_2 (011)[24] can result in significant continuum upshift of its VB edge, which improves the photocatalytic properties more effectively than traditional doping methods to create isolated midgap states. It appears, therefore, that the intrinsic defects in $B_{4.3}C$ play an

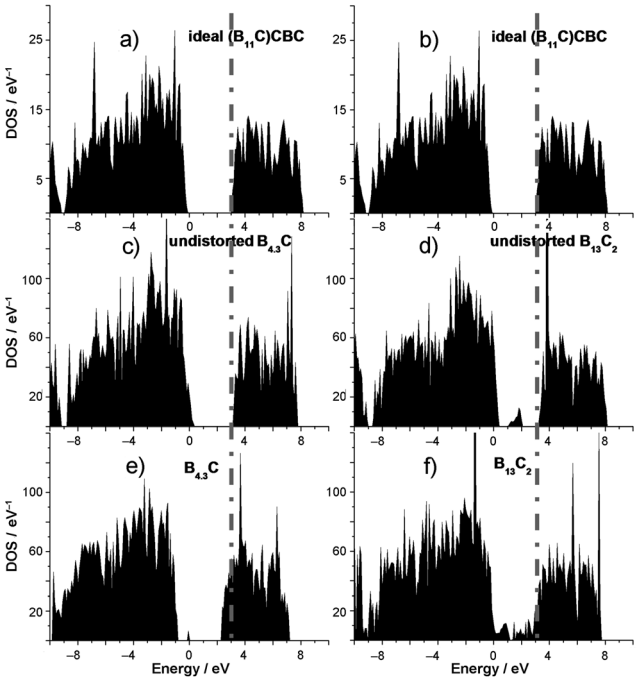

Figure 4. a) and b) Total density of states (DOS) of the optimized ideal structure of ($B_{11}C$)CBC. c) and d) The DOS of $B_{4.3}C$ and $B_{13}C_2$ with defects, but no structural relaxation. e) and f) The DOS of $B_{4.3}C$ and $B_{13}C_2$ with defects after structural relaxation. The dotted gray line highlights the downshift of the conduction band edge for $B_{4.3}C$.

important role in its effective photocatalysis under visible light irradiation.

The situation for $B_{13}C_2$ is slightly more complicated. Undistorted $B_{13}C_2$ exhibits many midgap states between the VB and CB because of its more complicated structural defects. In this case, the distortions in $B_{13}C_2$ introduce even more midgap states instead of downshifting the CB edge (Figure 4 f). It is well known that the midgap states can function as electron/hole traps and facilitate charge recombination,[25] and this may be one reason why $B_{13}C_2$ exhibits lower photocatalytic efficiency than $B_{4.3}C$.

In conclusion, two boron carbides have been demonstrated to perform photocatalytic H_2 evolution and PEC water reduction under visible light. Importantly, these metal-free photocatalysts exhibit high efficiency even without any precious metal cocatalyst loading. We further show that $B_{4.3}C$ exhibits better efficiency and stability than $B_{13}C_2$. DFT calculations suggest that the defects and structural distortions in $B_{4.3}C$ cause a downshift of its CB edge that narrows its band gap and facilitates its visible light absorption. However, in $B_{13}C_2$, the more complicated structural defects and distortions introduce midgap states between the CB and VB that facilitate charge recombination and reduce its photocatalytic efficiency. We expect that these boron carbides will provide new opportunities for the future development of efficient and stable visible-light-responsive photocatalysts and solar cell materials.

Experimental Section

The $B_{4.3}C$, labeled as "B_4C" on the bottle, was purchased from Alfa Aesar (CAS: 12069–32–8). The $B_{13}C_2$ was synthesized by arc-melting method. Typically, 26.3 g of crystalline boron reacts with 3.7 g of graphitic carbon under vacuum at 3100 °C by arc-melting for 2 min. The product was cast in a water-cooled hearth and cooled to room temperature. Materials shattered on cooling and were remelted by vacuum arc-melting and allowed to cool more slowly to inhibit shattering. The sintered bulky product was mashed into a powder by hammer, ball milling, and mortar/pestle milling. To remove possible impurities, such as boron oxides and transition metals, the boron carbide products were washed repeatedly with a sequence of HCl (2 M), distilled water, and ethanol. The materials were then dried in air at 70 °C overnight before use. Additional experimental details, including instrumental characterizations, DFT calculations, photocatalytic and PEC measurements, are given in the Supporting Information.

Received: November 23, 2012
Published online: January 28, 2013

Keywords: boron · carbides · hydrogen evolution · photocatalysis · water reduction

[1] a) X. Chen, S. Shen, L. Guo, S. S. Mao, *Chem. Rev.* **2010**, *110*, 6503–6570; b) A. Kudo, Y. Miseki, *Chem. Soc. Rev.* **2009**, *38*, 253–278; c) M. G. Walter, E. L. Warren, J. R. McKone, S. W. Boetcher, Q. Mi, E. A. Santori, N. S. Lewis, *Chem. Rev.* **2010**, *110*, 6446–6473.
[2] X. Wang, K. Maeda, A. Thomas, K. Takanabe, G. Xin, J. M. Carlsson, K. Domen, M. Antonietti, *Nat. Mater.* **2009**, *8*, 76–80.
[3] Y. Wang, X. Wang, M. Antonietti, *Angew. Chem.* **2012**, *124*, 70–92; *Angew. Chem. Int. Ed.* **2012**, *51*, 68–89.
[4] S. Yanagida, A. Kabumoto, A. L. Rheingold, D. M. Heinekey, *J. Chem. Soc. Chem. Commun.* **1985**, 474–475.
[5] Z. Zhang, J. Long, L. Yang, W. Chen, W. Dai, X. Fu, X. Wang, *Chem. Sci.* **2011**, *2*, 1826–1830.
[6] G. Liu, P. Niu, L. Yin, H. Cheng, *J. Am. Chem. Soc.* **2012**, *134*, 9070–9073.
[7] F. Wang, W. K. H. Ng, J. C. Yu, H. Zhu, C. Li, L. Zhang, Z. Liu, Q. Li, *Appl. Catal. B* **2012**, *111–112*, 409–414.
[8] Y. Hou, B. L. Abrams, P. C. K. Vesborg, M. E. Bjorketun, K. Herbst, L. Bech, A. M. Setti, C. D. Damsgaard, T. Pedersen, O. Hansen, J. Rossmeisl, S. Dahl, J. K. Norskov, L. Chorkendorff, *Nat. Mater.* **2011**, *10*, 434–438.
[9] a) C. Wood, D. Emin, *Phys. Rev. B* **1984**, *29*, 4582–4587; b) R. Lazzari, N. Vast, J. M. Besson, S. Baroni, A. Dal Corso, *Phys. Rev. Lett.* **1999**, *83*, 3230–3233.
[10] U. A. Joshi, A. Palasyuk, D. Arney, P. A. Maggard, *J. Phys. Chem. Lett.* **2010**, *1*, 2719–2726.
[11] K. A. Schwetz, P. Karduck, *AIP Conf. Proc.* **1990**, *231*, 405.
[12] a) U. Kuhlmann, H. Werheit, K. A. Schwetz, *J. Alloys Compd.* **1992**, *189*, 249–258; b) D. Emin, *Phys. Rev. B* **1988**, *38*, 6041–6055.
[13] H. Werheit, *J. Phys. Condens. Matter* **2006**, *18*, 10655–10662.
[14] a) H. Werheit, T. Au, R. Schmechel, S. O. Shalamberidze, G. I. Kalandadze, A. M. Eristavi, *J. Solid State Chem.* **2000**, *154*, 79–86; b) H. Werheit, H. W. Rotter, F. D. Meyer, H. Hillebrecht, S. O. Shalmberidze, T. G. Abzianidze, E. G. Esadze, *J. Solid State Chem.* **2004**, *177*, 569–574.
[15] D. Gosset, M. Colin, *J. Nucl. Mater.* **1991**, *183*, 161–173.
[16] F. Thévenot, *J. Eur. Ceram. Soc.* **1990**, *6*, 205–225.
[17] D. R. Tallant, T. L. Aselage, A. N. Campbell, D. Emin, *Phys. Rev. B* **1989**, *40*, 5649–5656.

[18] a) E. Amberger, W. Stumpf, K. C. Buschbeck, *Gmelin Handbook of Inorganic Chemistry*, Springer-Verlag, Berlin **1981**; b) M. Beauvy, *J. Less-Common Met.* **1983**, *90*, 169 – 175.
[19] J. E. Saal, S. Shang, Z. Liu, *Appl. Phys. Lett.* **2007**, *91*, 231915.
[20] D. M. Bylander, L. Kleinman, S. Lee, *Phys. Rev. B* **1990**, *42*, 1394 – 1403.
[21] a) P. Sarkar, P. S. Nicholson, *J. Am. Ceram. Soc.* **1996**, *79*, 1987 – 2002; b) A. R. Boccaccini, I. Zhitonirsky, *Curr. Opin. Solid State Mater. Sci.* **2002**, *6*, 251 – 260.
[22] V. Domnich, S. Reynaud, R. A. Haber, M. Chhowalla, *J. Am. Ceram. Soc.* **2011**, *94*, 3605 – 3628.
[23] X. Chen, L. Liu, P. Y. Yu, S. S. Mao, *Science* **2011**, *331*, 746 – 750.
[24] J. Tao, T. Luttrell, M. Batzill, *Nat. Chem.* **2011**, *3*, 296 – 300.
[25] J. H. Clark, M. S. Dyer, R. G. Palgrave, C. P. Ireland, J. R. Darwent, J. B. Claridge, M. J. Rosseinsky, *J. Am. Chem. Soc.* **2011**, *133*, 1016 – 1032.

